Zhang et al. *Zool. Res.* 2023, 44(6): 1003−1014
https://doi.org/10.24272/j.issn.2095-8137.2023.108

ZR | Zoological Research

Article Open Access

Anti-infection effects of heparin on SARS-CoV-2 in a diabetic mouse model

Zhongyun Zhang[1,2,#], Ning Zhang[3,#], Xuancheng Lu[4,#], Min Zhou[5], Xiaoxiang Yan[6], Weiqiong Gu[1,2], Jingru Yang[7], Qin Zhang[4], Cheng Zhang[3], Yuhuan Gong[3], Mingjun Jia[3], Xiaoyu Zhang[3], Peng Ning[3], Mei Liu[4], Xiaoyan Li[4], Xiaomeng Shi[4], Wenjun Liu[3,8], George F. Gao[3,4,8], Guang Ning[1,2], Jiqiu Wang[1,2,*], Yuhai Bi[3,7,8,*]

[1] *Department of Endocrinology and Metabolism*, *Shanghai Institute of Endocrine and Metabolic Diseases*, *Ruijin Hospital*, *Shanghai Jiao Tong University School of Medicine*, *Shanghai* 200025, *China*

[2] *Shanghai National Clinical Research Center for Metabolic Diseases*, *Key Laboratory for Endocrine and Metabolic Diseases of the National Health Commission of the PR China*, *Shanghai National Center for Translational Medicine*, *Shanghai* 200025, *China*

[3] *CAS Key Laboratory of Pathogen Microbiology and Immunology*, *Institute of Microbiology*, *Center for Influenza Research and Early-warning (CASCIRE)*, *CAS-TWAS Center of Excellence for Emerging Infectious Diseases (CEEID)*, *Chinese Academy of Sciences*, *Beijing* 100101, *China*

[4] *Laboratory Animal Center*, *Chinese Center for Disease Control and Prevention (China CDC)*, *Beijing* 102206, *China*

[5] *Department of Respiratory and Critical Care Medicine*, *Institute of Respiratory Diseases*, *Ruijin Hospital*, *Shanghai Jiao Tong University School of Medicine*, *Shanghai* 200025, *China*

[6] *Department of Cardiology*, *Institute of Cardiovascular Diseases*, *Ruijin Hospital*, *Shanghai Jiao Tong University School of Medicine*, *Shanghai* 200025, *China*

[7] *School of Laboratory Medicine and Life Sciences*, *Wenzhou Medical University*, *Wenzhou*, *Zhejiang* 325000, *China*

[8] *University of Chinese Academy of Sciences*, *Beijing* 100049, *China*

ABSTRACT

Severe acute respiratory syndrome coronavirus 2 (SARS-CoV-2) infection can result in more severe syndromes and poorer outcomes in patients with diabetes and obesity. However, the precise mechanisms responsible for the combined impact of coronavirus disease 2019 (COVID-19) and diabetes have not yet been elucidated, and effective treatment options for SARS-CoV-2-infected diabetic patients remain limited. To investigate the disease pathogenesis, K18-hACE2 transgenic (hACE2^{Tg}) mice with a leptin receptor deficiency (hACE2-Lepr$^{-/-}$) and high-fat diet (hACE2-HFD) background were generated. The two mouse models were intranasally infected with a 5×10^5 median tissue culture infectious dose ($TCID_{50}$) of SARS-CoV-2, with serum and lung tissue samples collected at 3 days post-infection. The hACE2-Lepr$^{-/-}$ mice were then administered a combination of low-molecular-weight heparin (LMWH) (1 mg/kg or 5 mg/kg) and insulin via subcutaneous injection prior to intranasal infection with 1×10^4 $TCID_{50}$ of SARS-CoV-2. Daily drug administration continued until the euthanasia of the mice. Analyses of viral RNA loads, histopathological changes in lung tissue, and inflammation factors were conducted. Results demonstrated similar SARS-CoV-2 susceptibility in hACE2^{Tg} mice under both lean (chow diet) and obese (HFD) conditions. However, compared to the hACE2-Lepr$^{+/+}$ mice, hACE2-Lepr$^{-/-}$ mice exhibited more severe lung injury, enhanced expression of inflammatory cytokines and hypoxia-inducible factor-1α (HIF-1α), and increased apoptosis. Moreover, combined LMWH and insulin treatment effectively reduced disease progression and severity, attenuated lung pathological changes, and mitigated inflammatory responses. In conclusion, pre-existing diabetes can lead to more severe lung damage

Received: 02 July 2023; Accepted: 04 September 2023; Online: 05 September 2023

Foundation items: This work was supported by the Strategic Priority Research Program of the Chinese Academy of Sciences (CAS) (XDB29010102); National Natural Science Foundation of China (NSFC) (91957124, 82161148010, 32041010); Self-supporting Program of Guangzhou Laboratory (SRPG22-001); National Science and Technology Infrastructure of China (National Pathogen Resource Center-NPRC-32); and Management Strategy of the Tertiary Prevention and Treatment of Diabetes Based on DIP system (supported by China Health Promotion Foundation). Y.B. was supported by the Youth Innovation Promotion Association of CAS (Y2021034) and Innovation Team and Talents Cultivation Program of the National Administration of Traditional Chinese Medicine (ZYYCXTD-D-202208)

#Authors contributed equally to this work

*Corresponding authors, E-mail: beeyh@im.ac.cn; wangjq@shsmu.edu.cn

upon SARS-CoV-2 infection, and LMWH may be a valuable therapeutic approach for managing COVID-19 patients with diabetes.

Keywords: SARS-CoV-2; Diabetes; Mouse model; Heparin; Antiviral therapy

INTRODUCTION

Coronavirus disease 2019 (COVID-19) caused by severe acute respiratory syndrome coronavirus 2 (SARS-CoV-2) remains a significant global health threat, accounting for hundreds of millions of infections and millions of deaths worldwide (https://covid19.who.int/) (Magiorkinis, 2023). While most COVID-19 patients experience mild to moderate respiratory illness and heal without specialized treatment (Verveen et al., 2022), certain cohorts, particularly older patients, and those with underlying medical conditions, such as diabetes, chronic respiratory disease, obesity, cardiovascular disease, and chronic kidney disease, can experience severe outcomes that require medical treatment (Nguyen et al., 2022; Zhang et al., 2022a). Recent retrospective studies have revealed that diabetes is one of the most common comorbidities in COVID-19 patients (Guan et al., 2020; Zhang et al., 2020a). Compared to non-diabetic patients, those with COVID-19 and diabetes face increased hospitalization rates, severe illness risks, and higher mortality rates (Kouidere et al., 2021; Zhang et al., 2021). Therefore, intensive monitoring and glucose-lowering therapies should be considered in COVID-19 patients with diabetes. Although the Chinese Clinical Guidance for COVID-19 Diagnosis and Treatment has been published (revised 10th edition; The Chinese National Health Commission, 2023), clinical guidelines for COVID-19 patients with diabetes have yet to be reported.

SARS-CoV-2 infection predisposes individuals to hypercoagulation and thrombotic complications, often leading to poor prognosis and necessitating intensive care regardless of the presence of diabetes (Abdi et al., 2022; Abou-Ismail et al., 2020; Abrignani et al., 2022; Desdiani, 2022). In addition, COVID-19 patients with pre-existing diabetes are more likely to develop severe or critical thromboembolic complications relative to those without diabetes (Petelina et al., 2022; Tang et al., 2020). However, the relationship between diabetes and SARS-CoV-2 infection-related symptoms, underlying pathogenic mechanisms in COVID-19 patients with diabetes, and effective treatment strategies have not been sufficiently studied.

Early in the pandemic, recommendations emerged suggesting the use of pharmacological thromboprophylaxis with low-molecular-weight heparin (LMWH) for all patients hospitalized with COVID-19, especially those with comorbidities such as diabetes, to mitigate thrombotic complications (De Vito et al., 2023). Compared to other oligosaccharides and glycosaminoglycans, LMWH can bind to various viruses as they traverse the extracellular matrix of the respiratory tract and demonstrates anticoagulant activity to prevent venous thromboembolism (Litov et al., 2021). A bidirectional relationship between coagulation and inflammation, as well as the anti-inflammatory and cytokine-reducing effects of LMWH, have been demonstrated in previous studies (Litov et al., 2021; Toor et al., 2021). However, the efficacy of LMWH for COVID-19 patients, including those with diabetes, remains untested in both clinical studies and animal models.

Human angiotensin-converting enzyme 2 (hACE2), the receptor for SARS-CoV-2, interacts with the spike (S) protein and mediates viral entry into cells (Dai et al., 2020; Shu et al., 2021; Zhou et al., 2020b). As mouse ACE2 does not interact with the SARS-CoV-2 S protein, mouse models are resistant to SARS-CoV-2 infection. Therefore, several transgenic mice expressing hACE2 have been engineered to study the pathogenic mechanism of SARS-CoV-2 infection and develop effective vaccines and drugs (Kim et al., 2022; Liang et al., 2020). K18-hACE2 mice expressing hACE2 driven by the cytokeratin 18 (*K18*) promoter are extremely susceptible to SARS-CoV-2, becoming severely ill (Arce & Costoya, 2021). These mice have been widely used to study the pathological basis of both mild and lethal SARS-CoV-2 infections and to assess potential therapeutic interventions. Hence, the hybrid descendants of K18-hACE2 and other disease mouse models (e.g., diabetes) could be used to investigate interactions between comorbidities and COVID-19. Type 2 diabetes mellitus is characterized by hyperphagia, obesity, hyperglycemia, and hyperinsulinemia. Leptin is the product of the mouse obese (*ob*) gene, and its receptor serves as a leptin signal (Huang et al., 2021; Jafari et al., 2022). Leptin-deficient (*ob/ob*) and leptin receptor-deficient (*db/db*) mice are hyperphagic and suffer from both obesity and type 2 diabetes mellitus (Oliveira et al., 2022; Rui et al., 2021).

In the current study, to examine the pathogenesis of severe disease caused by SARS-CoV-2 infection in patients with diabetes and to further explore the therapeutic effects of LMWH on comorbidities, we established two models based on K18-hACE2 mice. Homozygous leptin receptor-deficient mice ($hACE2^{Tg}Lepr^{-/-}$, abbreviated as hACE2-$Lepr^{-/-}$) and high-fat diet (HFD)-fed $hACE2^{Tg}Lepr^{+/+}$ (hACE2-$Lepr^{+/+}$) mice (hACE2-HFD) were prepared to mimic the complex pathological conditions of COVID-19 patients with diabetes and obesity.

MATERIALS AND METHODS

Clinical data source

A retrospective cohort of 475 patients suspected of having COVID-19 at Tongji Hospital (Wuhan, Hubei Province, China) from 10 February to 5 March 2020 was derived from published literature (Fan et al., 2020). The diagnostic criteria for COVID-19 were as follows: (1) fever or respiratory symptoms; (2) leukopenia or lymphopenia; and (3) computerized tomography (CT) scans showing features indicative of viral pneumonia with characteristic changes (Chung et al., 2020; Lei et al., 2020). Diagnosis of COVID‑19 required a positive result in either next-generation sequencing or quantitative real time polymerase chain reaction (qPCR) assays and more than two clinical criteria (Pascarella et al., 2020). After excluding 118 patients lacking RNA-based SARS-CoV-2 confirmation, 357 patients with confirmed COVID-19 were included in our analyses.

Virus

The SARS-CoV-2 strain hCoV-19/China/CAS-B001/2020 (CAS-B001) (National Microbiology Data Center NMDCN0000102-3, GISAID database EPI_ISL_514256-7), isolated and identified by Dr. Yuhai Bi's team, was used in this study.

Animals

Heterozygous leptin receptor-deficient mice ($Lepr^{+/-}$) on a

C57BLKS/J background and K18-hACE2 transgenic mice on a C57BL/6J background ($hACE2^{Tg}$), which express human ACE2 driven by the human epithelial cell cytokeratin-18 (*K18*) promoter, were purchased from Gempharmatech (Nanjing, China). To express hACE2 in *db/db* mice ($Lepr^{-/-}$), *in vitro* fertilization (IVF) was performed in $hACE2^{Tg}$ and $Lepr^{+/-}$ mice. Double heterozygous mice ($hACE2^{Tg}Lepr^{+/-}$) were then used for self-fertilization. Two strains of mice were obtained under this procedure, including heterozygous K18-hACE2 and homozygous leptin receptor-deficient mice ($hACE2^{Tg}Lepr^{-/-}$, abbreviated as hACE2-$Lepr^{-/-}$), and heterozygous K18-hACE2 and wild-type leptin-receptor mouse ($hACE2^{Tg}Lepr^{+/+}$, abbreviated as hACE2-$Lepr^{+/+}$, littermate controls). To construct the obesity mouse model, hACE2-$Lepr^{+/+}$ mice were randomly divided into a high-fat diet group (hACE2-HFD) and a chow diet group (hACE2-CD). In the HFD group, mice were fed a 60 kcal% HFD (Research Diet, 12492i) starting at 8–9 weeks old, resulting in hACE2-HFD mice displaying typical HFD features, such as obesity and significantly increased body weight. All mice had free access to water and were maintained on a 12 h day/night cycle in a temperature-controlled (23 ℃) and clean environment.

Ethics statement

All animal experiments involving live viruses were approved by the Ethics Committees of Institute of Microbiology, Chinese Academy of Sciences (IMCAS; Approval No. APIMCAS2020004) and were conducted according to the standard operating procedures for animal experimentation in an animal biosafety level 3 (ABSL-3) laboratory.

Animal challenge experiments

Eight male and six female 30-week-old hACE2-HFD mice were intranasally infected with a 5×10^5 median tissue culture infectious dose ($TCID_{50}$) of SARS-CoV-2 in 50 μL of phosphate-buffered saline (PBS). Three male and two female mice were euthanized 3 days post-infection (dpi) to measure viral loads, lung lesions, and inflammatory cytokine levels. The body weights of all mice were also monitored. Eight male and six female hACE2-CD mice were treated in the same manner as infection controls.

Ten 6-week-old hACE2-$Lepr^{-/-}$ mice were intranasally infected with 5×10^5 $TCID_{50}$ of SARS-CoV-2 in 50 μL of PBS. Four mice were euthanized at 3 dpi for measurement of viral loads, lung lesions, and inflammatory cytokine levels, while the remaining mice were monitored until the end of the experiment. Ten hACE2-$Lepr^{+/+}$ mice were treated in the same manner as infection controls.

According to different treatments with insulin glargine and LMWH, seventeen 7-week-old hACE2-$Lepr^{-/-}$ mice were divided into low-dose, high-dose, and saline groups. The low-dose group (n=6) was subcutaneously injected with 728 μg/kg insulin glargine and 1 mg/kg LMWH. The high-dose group (n=6) was subcutaneously injected with 728 μg/kg insulin glargine and 5 mg/kg LMWH. The saline group (n=5) was treated with saline as a control. Thirteen hACE2-$Lepr^{+/+}$ mice were divided into three groups in the same manner as hACE2-$Lepr^{-/-}$ mice, with five mice in the high-dose group, four mice in the low-dose group, and four mice in the saline group. The hACE2-$Lepr^{+/+}$ mice were subcutaneously injected with 5 mg/kg LMWH (high-dose group) or 1 mg/kg LMWH (low-dose group), as glucose levels in the hACE2-$Lepr^{+/+}$ mice were normal. At 1 h after drug treatment, all mice were intranasally infected with 1×10^4 $TCID_{50}$ of SARS-CoV-2 in 50 μL of PBS. All mice were treated with drugs or saline every day until euthanized at 3 dpi.

Daily monitoring and sample collection

Clinical manifestations, body weight, blood glucose levels, dietary intake, and excretion output were recorded daily post-challenge until sacrifice at 3 dpi. Approximately half of the lung tissues were fixed in 4% (v/v) paraformaldehyde for histopathological analysis using hematoxylin-eosin (H&E) staining and immunohistochemistry (IHC). The remaining lung and trachea tissues were weighed and homogenized for RNA extraction and virus detection using qPCR. Tail blood glucose levels were measured using a ONETOUCH UltraEasy glucometer and glucose test strips (Johnson & Johnson Medical China, China).

Viral RNA detection

Viral RNA was extracted from lung lysates using a QIAamp Viral RNA Kit (Qiagen, Germany) and the virus was detected using a COVID-19 virus (2019-nCoV) Triple-Detection Kit (real-time PCR) (Mabsky Bio-Tech, China) according to the manufacturer's instructions. The PCR procedure was performed as described previously (Wang et al., 2021).

H&E staining and histological analysis

Lung tissues were fixed with 4% paraformaldehyde at 23–25 ℃ overnight, then dehydrated, paraffin-embedded, and sectioned (5 μm), followed by deparaffinization and H&E staining. To assess pathological changes in the lung tissues, each H&E-stained section was scored using panoramic scan images in Case Viewer by one independent observer blind to the experimental conditions according to International Harmonization of Nomenclature and Diagnostic Criteria (INHAND) (https://www.toxpath.org/inhand.asp) (Fan et al., 2022).

Immunohistochemical staining

Here, IHC analysis was performed using specific monoclonal antibodies for SARS-CoV-2 nucleocapsid (1:3 000, 40143-R001, SinoBiological, China), F4/80 (1:1 000, 70076; Cell Signaling Technology, USA), and hypoxia-inducible factor-1α (HIF-1α; 1:200, 20960-1-AP; Proteintech, China). IHC staining was performed using a REAL™ EnVision™ system (K5007; DAKO, Denmark). Paraffin sections were deparaffinized in xylene (three times, 20 min each), then rehydrated in descending grades of ethanol, followed by distilled water for 5 min. The sections were incubated in hydrogen peroxide (100 μL) for 10 min and rinsed in PBS (three times, 5 min each). For antigen repair, the slices were placed in ethylenediaminetetraacetic acid (EDTA, E9884; Sigma, USA) pH 9.0 buffer and microwaved on medium heat for 15 min and low heat for 15 min before power failure. The slides were rinsed in PBS (three times, 5 min each) and blocked with 5% bovine serum albumin (BSA, B2064; Sigma, USA) in PBS (blocking solution) for 20 min. The slides were washed briefly once with PBS to remove BSA, incubated with 100 μL of primary antibody diluted specifically for each section overnight at 4 °C, rinsed in PBS (three times, 5 min each), incubated with 100 μL of secondary antibody diluted specifically for each section for 30 min at room temperature, and rinsed with PBS (three times, 5 min each). Substrate-chromogen mixture (100 μL) was applied to each section and incubated at room temperature for 3–10 min, then rinsed with distilled water. The slides were counterstained with hematoxylin for 1 min, differentiated with 1% hydrochloric acid alcohol for 30 s,

dehydrated with descending grades of ethanol, and mounted with neutral tree gum. Tissue staining results of F4/80, and HIF-1α were observed and recorded under a light microscope using TissueFAXS viewer. SARS-CoV-2 nucleocapsid staining was observed using a 3DHISTECH Slide Converter. Brown granules in cells represented positive signals.

Immunofluorescence assay

Apoptosis was assessed using terminal deoxynucleotidyl transferase deoxyuridine triphosphate nick-end labeling (TUNEL) staining with an *In Situ* Cell Death Detection Kit (11684795910; Roche, Switzerland). Paraffin sections were deparaffinized in xylene (three times, 10 min each), then rehydrated in descending grades of ethanol and placed in distilled water for 5 min. After washing in Tris-buffered saline (three times, 5 min each), the sections were treated with 20 μg/mL proteinase K (ST532; Beyotime, China). The sections were washed with Tris-buffered saline and incubated with 50 μL of TUNEL reaction mixture at 37 °C for 1 h. The sections were then counterstained with Fluoroshield containing DAPI (ab104139; Abcam, UK) for 10 min at room temperature and visualized using a fluorescence microscope (Nikon, Japan).

Cytokine detection

Total RNA was extracted from lung lysates using a QIAamp Viral RNA Kit (Qiagen, Germany) according to a manufacturer's instructions. RNA concentration was determined using a NanoDrop 2000 spectrophotometer (Thermo Fisher Scientific, USA). cDNA was synthesized from RNA using a HiScript III 1st Strand cDNA Synthesis Kit (Vazyme, China) according to the manufacturer's instructions. Genomic DNA was eliminated using 2 μL of 5×gDNA wiper Mix and 1 μg of total RNA at 42 °C for 2 min. The mixture (10 μL) and 10×RT Mix (2 μL), HiScript III Enzyme Mix (2 μL), Oligo $(dT)_{20}VN$ (1 μL), random hexamers (1 μL), and RNase-free ddH_2O (4 μL) were added in a RNase-free tube for cDNA synthesis. The synthesis reaction for cDNA was as follows: 37 °C for 15 min, 85 °C for 5 s. The cDNA was applied for qPCR using the SYBR Green method with ChamQ Universal SYBR qPCR Master Mix (Vazyme, China). All qPCR procedures were performed using the ABI 7500 Fast Real-Time PCR System (USA) on 96-well plates. Gene expression fold-changes were calculated using the $2^{-\Delta\Delta Ct}$ method in Microsoft Excel. Primer sequences used included: IL-1β (Forward: 5'-CCGTGGACCTTCCAGGATGA-3'; Reverse: 5'-GGGAACGTCACACACCAGCA-3'); IFN-γ (Forward: 5'-AGCC ACGGAGAGTCAATGG-3'; Reverse: 5'-GCTCTGACACG AAACTGTGTTTT-3'); CXCL-10 (Forward: 5'-CCAAGT GCTGCCGTCATTTTC-3'; Reverse: 5'-GGCTCGCAGGGA TGATTTCAA-3'), and β-actin (Forward: 5'- ATGGCCA GGTCATCACCATTG-3'; Reverse: 5'- CAGGAAGGAAG GCTGGAAAAG-3').

Statistical analysis

Patients with COVID-19 were divided into non-diabetic and diabetic groups based on medical history. Descriptive statistics for all study variables were evaluated. Continuous numerical variables were expressed as mean±standard deviation (*SD*) or median with interquartile range (IQR). Categorical variables were expressed as counts with frequencies (percentages). Student's *t*-test or Mann-Whitney Wilcoxon test for continuous variables and chi-squared test or Fisher's exact test for categorical variables were used for comparisons between two groups. A univariate logistic regression model was used to calculate the influence of fasting blood glucose (FBG) on the incidence of symptoms and complications in patients with COVID-19. A multivariate logistic regression model was used to control for the influence of covariates, including age, hypertension, and coronary heart disease, on the incidence of symptoms and complications in patients with COVID-19. Results were expressed as an odds ratio (OR) with 95% confidence interval (CI). A *P*-value of less than 0.05 was set as the threshold for determining statistically significant differences. All statistical analyses were two-sided and performed using SPSS v26 software (SPSS, USA).

Statistical analyses of H&E scores, IHC scores, and cytokine levels were performed using GraphPad Prism v8.0 (GraphPad, USA). Statistical significance among different groups was determined using Student's *t*-test, and differences between experimental groups were considered statistically significant at $P<0.05$.

RESULTS

Correlation between diabetes and SARS-CoV-2 infection-related symptoms

A total of 357 patients with COVID-19 (190 males and 167 females) from Wuhan, China, were included in this study (Fan et al., 2020). Patients with diabetes showed higher levels of FBG (7.35, IQR 5.89–9.85 mmol/L vs. 5.45 IQR 4.96–6.67 mmol/L; $P<0.001$). Compared to the non-diabetic group, patients with diabetes were more likely to have comorbidities, including hypertension (59.1% vs. 31.6%; $P<0.001$) and coronary heart disease (21.2% vs. 9.3%; $P=0.006$). Regarding the main symptoms of COVID-19, the incidence of expectoration was higher in the diabetic group than in the non-diabetic group (66.7% vs. 52.6%; $P=0.038$). Upon admission, patients with diabetes showed lower oxygen saturation (SpO_2; 96.00, IQR 92.00%–98.00% vs. 97.00, IQR 95.00%–99.00%; $P=0.018$) and a higher respiratory rate (RR; 20.00, IQR 20.00–22.00 beat per minute (bpm) vs. 20.00, IQR 18.00–20.00 bpm; $P=0.048$) compared to non-diabetic patients. Other characteristics did not differ between the two groups (Supplementary Tables S1, S2).

In the univariate logistic regression model, a high FBG was a risk factor for the incidence of several complications, including respiratory failure (OR=1.11, 95% CI 1.03–1.21, $P=0.012$), acute respiratory distress syndrome (OR=1.15, 95% CI 1.06–1.24, $P<0.001$), acute myocardial injury (OR=1.10, 95% CI 1.02–1.18, $P=0.009$), acute kidney injury (OR=1.14, 95% CI 1.06–1.24, $P=0.001$), and septic shock (OR=1.11, 95% CI 1.02–1.20, $P=0.016$). Notably, hyperglycemia was also a risk factor for mortality (OR=1.18, 95% CI 1.09–1.29, $P=0.001$). After adjusting for age, hypertension, and coronary heart disease with the multivariable logistic regression model, a high FBG remained a significant risk factor affecting the incidence of respiratory failure (OR=1.10, 95% CI 1.00–1.20, $P=0.041$), acute respiratory distress syndrome (OR=1.12, 95% CI 1.04–1.21, $P=0.003$), and acute kidney injury (OR=1.11, 95% CI 1.03–1.20, $P=0.006$). Additionally, a high FBG remained a significant risk factor for mortality (OR=1.15, 95% CI 1.06–1.24, $P=0.001$). However, FBG was not associated with the incidence of primary COVID-19 symptoms based on univariate and multivariable logistic regression analyses (Supplementary Table S3).

hACE2-transgenic mice are sensitive to SARS-CoV-2 infection under CD and HFD

K18-hACE2-transgenic ($hACE2^{Tg}$) mice were fed with a HFD or CD for comparative analysis. The non-FBG levels in male and female hACE2-HFD mice (mean values of 12.7 and 12.9 mmol/L, respectively) were slightly higher than those in hACE2-CD mice (10.0 and 11.0 mmol/L, respectively) at 0 and 3 dpi. Blood glucose levels markedly decreased at 3 dpi compared to levels at 0 dpi (Figure 1A), which may be related to anorexia in mice after infection.

Following infection with SARS-CoV-2 at a high virus titer of 5×10^5 $TCID_{50}$, all hACE2-HFD and hACE2-CD male and female mice exhibited signs of depression, delayed responses, reduced body weights, and clustering behavior, and all died by 5 dpi. Interestingly, hACE2-HFD mice showed lower body weight losses (10.0% in both male and female mice) compared to male and female hACE2-CD mice (17.7% and 18.6%, respectively) (Figure 1B), which may be due to slow fat metabolism under the HFD in hACE2-HFD animals.

The mice were euthanized at 3 dpi, and lung virus titers (viral RNA copies) were tested using qPCR targeting the *N, ORF1ab*, and *S* genes. Results revealed no significant differences between the hACE2-HFD and hACE2-CD mice (Figure 1C). However, female mice presented higher positive areas of SARS-CoV-2 nucleoprotein (N protein) in IHC staining compared to CD-fed male mice, but the opposite in the HFD-fed groups. In addition, male mice in the HFD group presented higher positive areas compared to those in the CD group (Figure 1D, E).

H&E staining showed that all four groups had interstitial pneumonia with widened alveolar septum, inflammatory cell infiltration, and diffuse alveolar damage (Figure 1F). Although female mice tended to show higher H&E scores than males in both the CD and HFD groups, the differences were not significant (Figure 1G). Additionally, the lung tissue in all groups was infiltrated with macrophages, as indicated by F4/80 staining (Supplementary Figure S1). HIF-1α, as a core regulator of hypoxic signaling, was highly stained in the lungs in both male and female mice in the CD and HFD groups, particularly in the bronchi (Figure 1H). Positive TUNEL signals indicating apoptosis were detected in all groups, particularly in male HFD mice (Figure 1I). These data indicate that $hACE2^{Tg}$ mice are relatively sensitive to SARS-CoV-2, resulting in lung damage with hypoxia and apoptosis, whereas HFD-induced obesity and mild elevation in blood glucose did not significantly aggravate infection in this mouse model.

hACE2-Lepr$^{-/-}$ mice exhibit more severe symptoms after SARS-CoV-2 infection

Diabetic mice, including *ob/ob* and *db/db* mice, are often applied as diabetic models as their clinical symptoms closely resemble those of diabetics. Here, hACE2-Lepr$^{-/-}$ mice were constructed as the diabetic model by hybridization with leptin receptor-deficient (*db/db*) and $hACE2^{Tg}$ mice to evaluate disease progression and pathogenesis of SARS-CoV-2 infection. After infection with 5×10^5 $TCID_{50}$ of SARS-CoV-2, body weights were monitored each day of the experiment, with blood and lung samples collected at 3 dpi (Figure 2A). After infection, mice in the hACE2-Lepr$^{-/-}$ and hACE2-Lepr$^{+/+}$ groups showed obvious clinical manifestations, such as dyspnea, with hemoptysis observed in several hACE2-Lepr$^{-/-}$ mice. Mice in both groups showed decreased body weights after infection, with lower body weights in the hACE2-Lepr$^{-/-}$ group compared to the hACE2-Lepr$^{+/+}$ group at 1 dpi (Figure 2B). All mice (10/10) died before 4 dpi in both groups, although the mean death time in the hACE2-Lepr$^{-/-}$ group (2.5 days) was shorter than that in the hACE2-Lepr$^{+/+}$ group (3.6 days) (Figure 2C).

The hACE2-Lepr$^{-/-}$ mice showed extreme hyperglycemia, reaching the upper detection limit of 35 mmol/L at 3 dpi, which was significantly higher than that in the control mice with a normal blood glucose range (Figure 2D). In addition, higher lung viral load (RNA copies) (Figure 2E) and stronger SARS-CoV-2 N protein positive signals in the lung were detected in the hACE2-Lepr$^{-/-}$ group compared to the hACE2-Lepr$^{+/+}$ group, although the differences were not significant (Figure 2F-H). Moreover, more severe histological changes with higher scores were observed in the hACE2-Lepr$^{-/-}$ group at 3 dpi (Figure 2G, H).

Obvious macrophage infiltration was observed in the lungs of both groups, with no significant difference observed between the groups (Supplementary Figure S2). Stronger positive HIF-1α signals in the alveolus were observed in the hACE2-Lepr$^{-/-}$ mice compared to the hACE2-Lepr$^{+/+}$ mice, indicating more severe dyspnea (Figure 2I). Positive TUNEL signals were extensively observed in the alveoli and bronchi of hACE2-Lepr$^{-/-}$ mice, suggesting marked apoptosis, whereas few positive signals were detected in the hACE2-Lepr$^{+/+}$ mice (Figure 2J). These results indicate that alveolar and bronchial cell damage and death occurred at an early stage of viral infection, resulting in hypoxic changes and dyspnea symptoms under diabetic conditions.

Heparin alleviates SARS-CoV-2 infection in hACE2-Lepr$^{-/-}$ mice

Hypercoagulative states and thrombotic events are important features of patients with COVID-19 (Abrignani et al., 2022; Abou-Ismail et al., 2020). Given the anticoagulant properties of heparin and its frequent application in thrombotic disease treatments (Di Micco et al., 2021), the therapeutic effects of heparin were evaluated in COVID-19 patients with diabetes. As the high dose of 5×10^5 $TCID_{50}$ of virus caused high lethality, we reduced the infection dose to 1×10^4 $TCID_{50}$. Heparin and insulin were administered to hACE2-Lepr$^{-/-}$ mice, while only heparin was administered to hACE2-Lepr$^{+/+}$ mice. Results showed no significant differences in body weight loss in the hACE2-Lepr$^{+/+}$ mice among the saline, low-dose heparin (1 mg/kg), and high-dose heparin (5 mg/kg) treatment groups before 3 dpi. However, the infected hACE2-Lepr$^{-/-}$ mice treated with high-dose heparin showed an apparently slower rate of weight loss compared to those in the low-dose heparin and saline control groups (Figure 3A). The hACE2-Lepr$^{+/+}$ mice maintained relatively stable blood glucose levels in the control and heparin-treated groups after infection, whereas the hACE2-Lepr$^{-/-}$ mice showed fluctuating blood glucose levels, tending to become stable after heparin and insulin administration, particularly in the high dose group (5 mg/kg heparin) compared to the control group (saline) (Figure 3B). Interestingly, the blood glucose values increased sharply in all hACE2-Lepr$^{-/-}$ mice on 3 dpi (Figure 3B), which may be attributed to ketone metabolism as a secondary effect of virus infection (Ramos-Guzman et al., 2021).

Following SARS-CoV-2 infection, all hACE2-Lepr$^{+/+}$ and hACE2-Lepr$^{-/-}$ mice treated with a high dose of heparin displayed reduced viral loads (virus RNA copies) compared to the corresponding controls without heparin treatment (Figure 3C). In addition, rare positive signals for the viral N

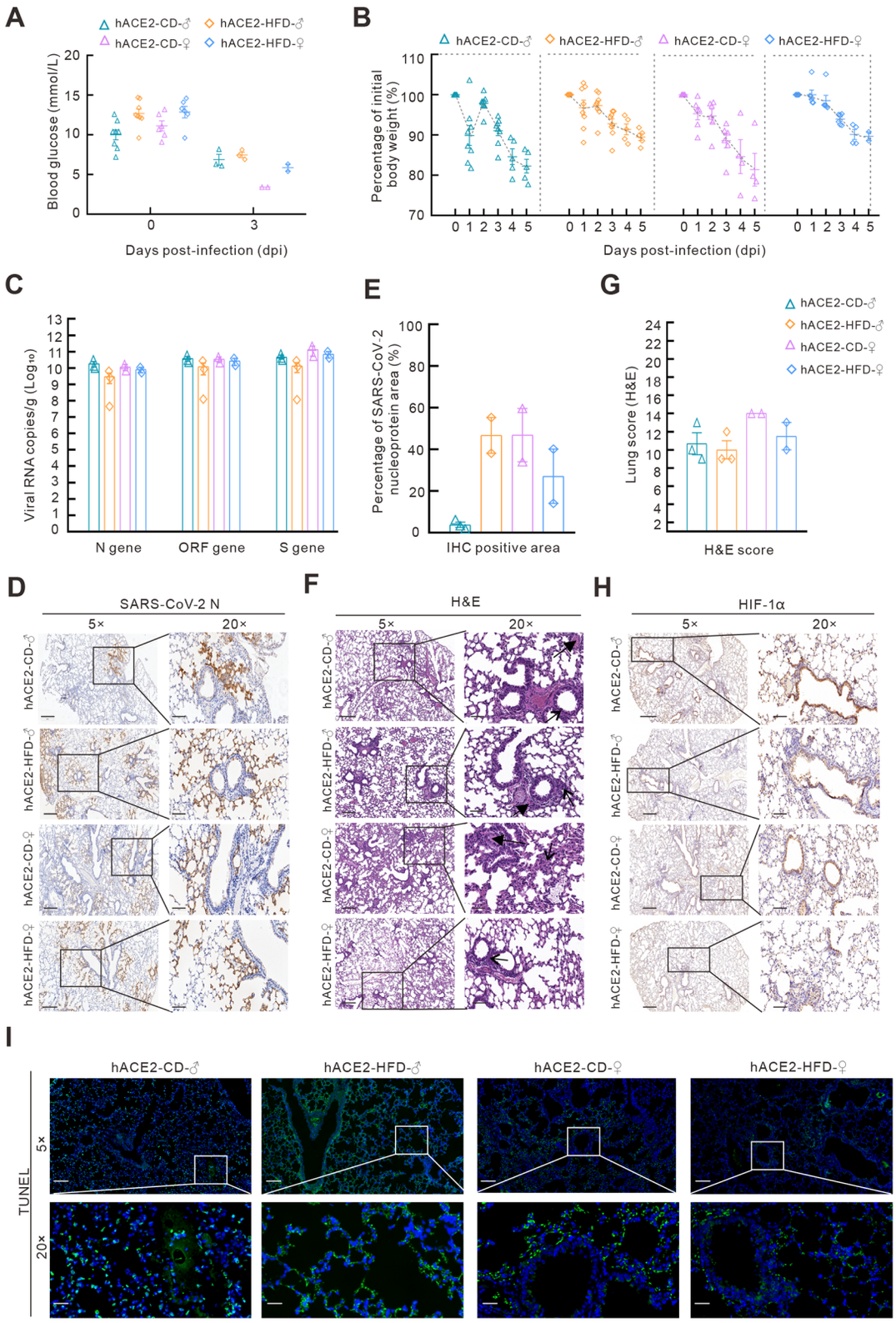

Figure 1 hACE2-transgenic mice are sensitive to SARS-CoV-2 infection under both CD and HFD

A, B: Blood glucose levels (A) and body weight changes (B) in hACE2-transgenic mice (hACE2^{Tg}) fed CD or HFD after SARS-CoV-2 infection. C: SARS-CoV-2 *N*, *ORF1ab*, and *S* genes were detected using qPCR in the lungs of hACE2-CD and hACE2-HFD mice after infection. D: SARS-CoV-2 N proteins in the lungs were detected using IHC. 5×, scale bar represents 400 μm; 20×, scale bar represents 100 μm. E: SARS-CoV-2 N protein-positive area was calculated using Case Viewer. F: Histopathological changes associated with SARS-CoV-2 infection in lung tissues of hACE2-CD and hACE2-HFD mice detected using H&E staining (arrow indicates inflammatory cell infiltration, bold arrow indicates hyaline membrane). 5×, scale bar represents 200 μm; 20×, scale bar represents 50 μm. G: Lung scores were counted according to INHAND standard rules. H: HIF-1α expression in lungs of hACE2-CD and hACE2-HFD mice after infection was detected using IHC. I: TUNEL immunofluorescence staining of lungs in hACE2-CD and hACE2-HFD mice. H, I: Shown at 5×, scale bar represents 300 μm; 20×, scale bar represents 100 μm.

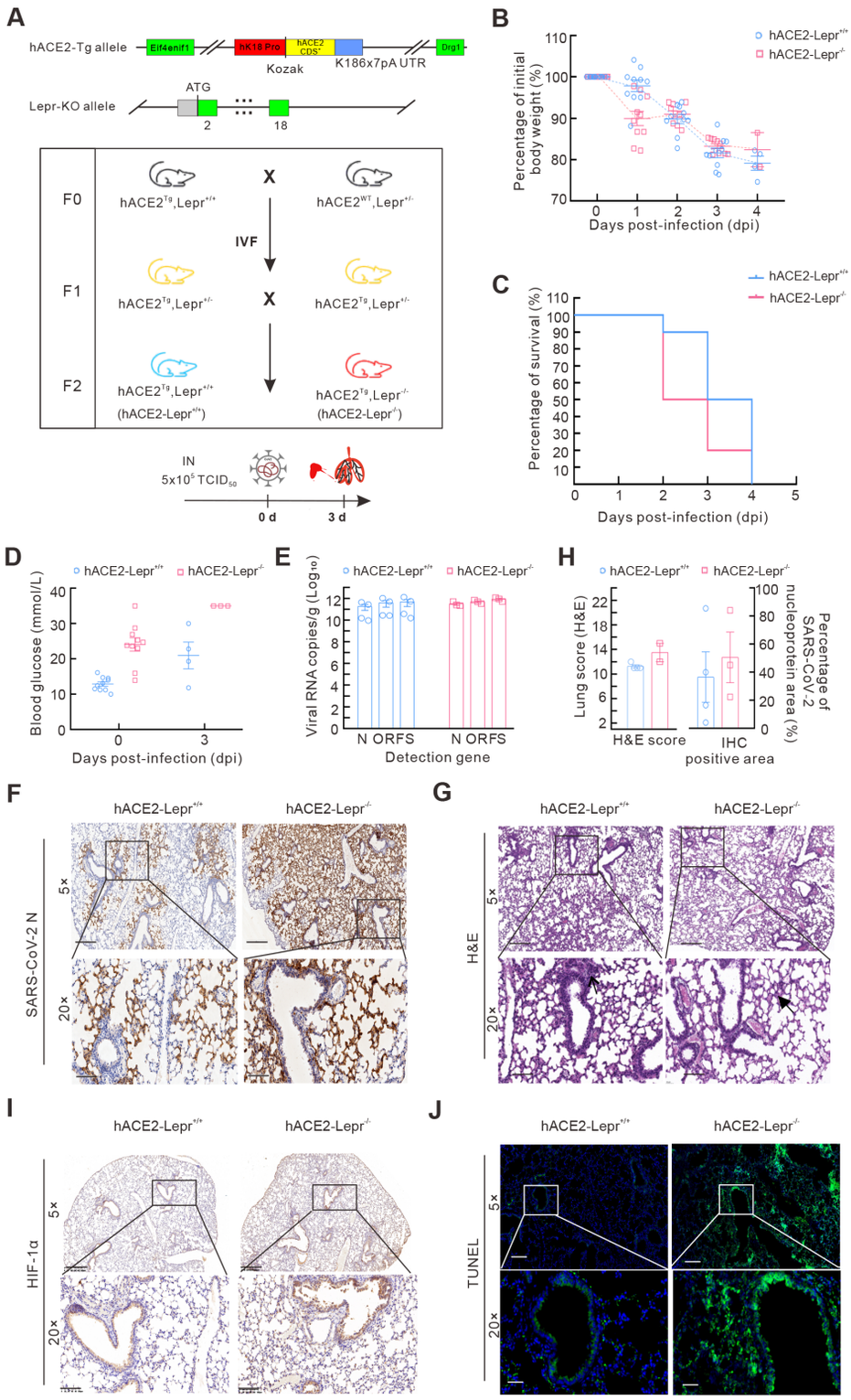

Figure 2 Diabetic mice show more severe symptoms after SARS-CoV-2 infection

A: Schematic of hACE2-Lepr$^{-/-}$ mouse model construction and challenge procedures. B, C: Body weight changes (B) and survival rates (C) of hACE2-Lepr$^{-/-}$ and hACE2-Lepr$^{+/+}$ mice after SARS-CoV-2 infection. D: Blood glucose levels in hACE2-Lepr$^{-/-}$ and hACE2-Lepr$^{+/+}$ mice before and after infection. E: SARS-CoV-2 *N*, *ORF1ab*, and *S* gene levels in lungs of hACE2-Lepr$^{-/-}$ and hACE2-Lepr$^{+/+}$ mice were detected by qPCR. F: IHC assay of SARS-CoV-2 N protein in lungs of hACE2-Lepr$^{-/-}$ and hACE2-Lepr$^{+/+}$ mice after virus infection. 5×, scale bar represents 400 μm; 20×, scale bar represents 100 μm. G: Histopathological changes in lung tissues of hACE2-Lepr$^{-/-}$ and hACE2-Lepr$^{+/+}$ mice after virus infection (arrow indicates inflammatory cell infiltration, bold arrow indicates hyaline membrane). 5×, scale bar represents 200 μm; 20×, scale bar represents 50 μm. H: Lung pathological (H&E) scores (left) were counted according to INHAND standard rules, and SARS-CoV-2 N protein-positive area (right) was calculated using Case Viewer. I: IHC assay for HIF-1α in lungs of hACE2-Lepr$^{-/-}$ and hACE2-Lepr$^{+/+}$ mice after infection. J: TUNEL immunofluorescence staining of lungs in hACE2-Lepr$^{-/-}$ and hACE2-Lepr$^{+/+}$ mice. I, J: Shown at 5×, scale bar represents 300 μm; 20×, scale bar represents 100 μm.

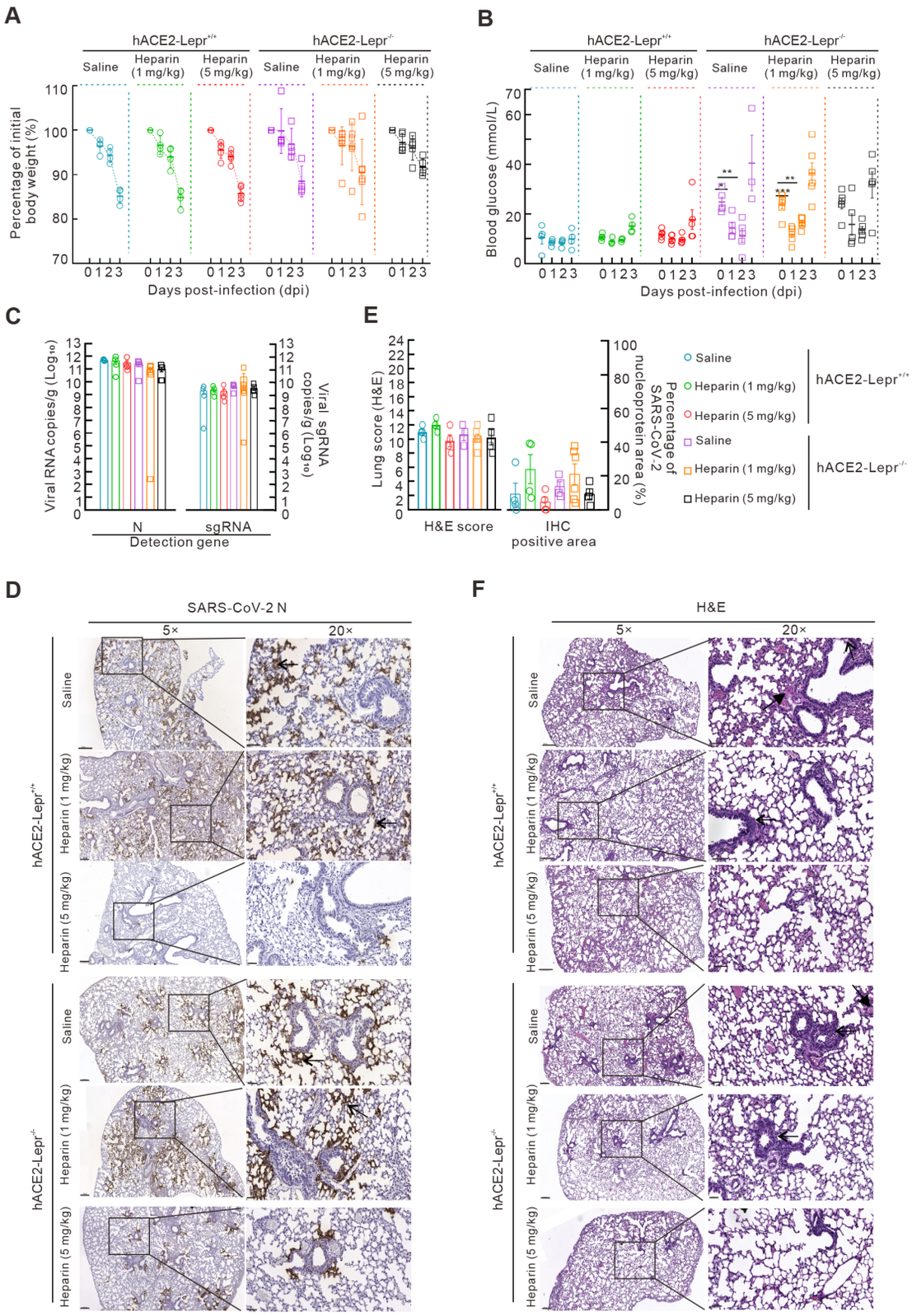

Figure 3 Heparin alleviates SARS-CoV-2 infection in diabetic models

A, B: Body weight changes (A) and blood glucose levels (B) in hACE2-Lepr$^{-/-}$ and hACE2-Lepr$^{+/+}$ mice infected by 1×10^4 $TCID_{50}$ of SARS-CoV-2 and treated with low-dose (1 mg/kg) and high-dose (5 mg/kg) heparin. C: SARS-CoV-2 *N* gene and sub-gene levels were detected using qPCR in the lungs of hACE2-Lepr$^{-/-}$ and hACE2-Lepr$^{+/+}$ mice treated with drugs. D: IHC assay for SARS-CoV-2 N proteins in lungs of hACE2-Lepr$^{-/-}$ and hACE2-Lepr$^{+/+}$ mice treated with heparin. 5×, scale bar represents 400 μm; 20×, scale bar represents 100 μm. E: Lung pathological (H&E) scores (left) were counted according to INHAND standard rules, and SARS-CoV-2 N protein-positive area (right) was calculated using Case Viewer. F: Histopathological changes in lung tissues of hACE2-Lepr$^{-/-}$ and hACE2-Lepr$^{+/+}$ mice treated with drugs (arrow indicates inflammatory cell infiltration, bold arrow indicates hyaline membrane). 5×, scale bar represents 200 μm; 20×, scale bar represents 50 μm.

protein were detected in hACE2-Lepr$^{+/+}$ and hACE2-Lepr$^{-/-}$ mice treated with high-dose heparin (Figure 3D, E) compared to signals in the control and low-dose heparin-treated mice, in which abundant positive signals for the viral N protein were detected in alveolar and bronchiolar epithelial cells in the lungs. H&E staining revealed diffuse bronchial destruction, hyaline membrane formation, protein-rich effusion, inflammation cell infiltration, and alveolar collapse with hemorrhage in the lungs of control hACE2-Lepr$^{+/+}$ and hACE2-Lepr$^{-/-}$ mice (Figure 3F). In comparison, mice treated with heparin, especially those in the high-dose group, showed reduced pathological scores, minimal inflammatory cell infiltration, and mild alveolar septum thickening in the lungs (Figure 3E, F). Thus, high-dose heparin (5 mg/kg) appears to alleviate lung damage caused by SARS-CoV-2 infection in normal and diabetic mice.

Concurrent with the heightened severity of infection in hACE2-Lepr$^{-/-}$ mice, abundant positive signals for the HIF-1α protein were detected in their lungs. In contrast, HIF-1α expression was reduced after high-dose heparin treatment (Figure 4A). Inflammatory cytokines and chemokines associated with SARS-CoV-2 infection (Polidoro et al., 2020) were also detected. After SARS-CoV-2 infection, C-X-C chemokine ligand 10 (CXCL-10) expression was markedly elevated (~80-fold higher) in the hACE2-Lepr$^{-/-}$ mice compared to that in the uninfected control mice but decreased by nearly half (~40-fold higher) after heparin treatment (Figure 4B). Interestingly, CXCL-10 expression in the infected hACE2-Lepr$^{+/+}$ mice was mildly elevated (~7.5-fold) compared to that in the uninfected control mice. This increased to ~15-fold and ~20-fold after administration of low- and high-dose heparin, respectively, suggesting that heparin regulates CXCL-10 expression, which further mediates inflammatory reactions after infection (Glaser et al., 2006). Interferon γ (IFN-γ) expression also increased in SARS-CoV-2-infected hACE2-Lepr$^{+/+}$ and hACE2-Lepr$^{-/-}$ mice, although relative elevations were lower in hACE2-Lepr$^{-/-}$ mice, but decreased after heparin treatment (Figure 4B). Interleukin-1β (IL-1β) expression was also decreased in both SARS-CoV-2-infected hACE2-Lepr$^{+/+}$ and hACE2-Lepr$^{-/-}$ mice following heparin treatment (Figure 4B). Collectively, these findings suggest that SARS-CoV-2 infection induces overexpression of pro-inflammatory factors such as CXCL-10 as well as hypoxia associated with HIF-1α expression. Importantly, heparin alleviates the pathological effects observed in the diabetic model.

DISCUSSION

Recent investigations (Singh & Khunti, 2022; Wang et al., 2020; Zhou et al., 2020a), as well as our retrospective cohort study, indicate that COVID-19 patients with diabetes and obesity are at a higher risk of severe disease and mortality. However, the etiological and pathophysiological mechanisms underpinning the heightened risk of complications in diabetic patients with COVID-19 remain unclear. Here, we constructed obesity and diabetes mouse models based on a hACE2^{Tg} background. Notably, hACE2^{Tg} mice were susceptible to SARS-CoV-2 infection and displayed comparable disease severity under both HFD and CD feeding regimes. This could be attributed to the marginal increase in blood glucose in the HFD-fed mice and high sensitivity of hACE2^{Tg} mice to SARS-CoV-2 infection. Similarly, hACE2^{Tg} mice with the K18 promotor are also reported to be extremely sensitive to SARS-CoV-2 (Arce & Costoya, 2021). The body weights of the hACE2^{Tg} mice fed a HFD for 22 weeks reached approximately 55 g, two-fold higher than that of the CD group, suggesting that obesity may not be a critical factor influencing severity of SARS-CoV-2 infection. Nevertheless, the precise effects of varying obesity levels on disease progression and severity post SARS-CoV-2 infection should be further investigated. Additionally, hACE2-Lepr$^{-/-}$ mice with homozygous leptin receptor deficiency showed high blood glucose levels and severe disease after SARS-CoV-2 infection, similar to the characteristics in severe and critical human COVID-19 cases. These observations support the postulated relationship between blood glucose levels and disease severity post SARS-CoV-2 infection (Lima-Martinez et al., 2021).

SARS-CoV-2 infection is associated with acute respiratory distress and hypoxia (Francistiova et al., 2021). Furthermore, respiratory failure and acute inflammatory reactions have also been observed in severe and critical COVID-19 cases (Merad et al., 2022; Santus et al., 2020). HIF-1α functions as a key regulator of physiological functions and is an important activator of glycolysis and the inflammatory response (Dong et al., 2022; Zepeda et al., 2013). Given that glycolysis primarily occurs under anoxic conditions, HIF-1α can serve as an indicator of dyspnea, especially after infection (Ou & Lv, 2020). We previously showed that cellular metabolism switches from oxidative phosphorylation to glycolysis in a human lung organoid model within 2 days of SARS-CoV-2 infection (Wang et al., 2021). In the current study, SARS-CoV-2-infected hACE2-Lepr$^{+/+}$ and hACE2-Lepr$^{-/-}$ mice exhibited markedly increased expression of HIF-1α, indicating the occurrence of dyspnea. Apoptosis also plays a pivotal role in the pathological features induced by SARS-CoV-2 infection (Zhu et al., 2020). Previous studies have shown that SARS-CoV-2 infection can induce acute lung injury and subsequent apoptosis in hamsters (O'Donnell et al., 2021), while antihistamines and remdesivir in combination can effectively alleviate inflammation-related injury in mice infected with the SARS-CoV-2 variant B.1.351 (Wu et al., 2022). Of note, the detection of apoptosis signals in both these animal models corroborates the suitability of our mouse models for investigating the pathogenic mechanisms underlying SARS-CoV-2 infection.

HIF-1α is commonly induced in acute inflammation microenvironments (Abdelmassih et al., 2021). Several studies have demonstrated that HIF-1α plays an essential role in SARS-CoV-2 infection and is necessary for creating a proinflammatory state (Tian et al., 2021; Wang et al., 2022). Here, we detected increased CXCL-10 and IFN-γ expression in the hACE2-Lepr$^{+/+}$ and hACE2-Lepr$^{-/-}$ mice, consistent with observations in COVID-19 patients (Polidoro et al., 2020). CXCL-10 is a proinflammatory cytokine and small secretory immune modulator of the immune response by the recruitment of leukocytes, including monocytes, T cells, and macrophages (Javeed et al., 2021). IFN-γ is highly up-regulated in severe COVID-19 patients, and is critical for inflammatory cell death, inflammation, tissue and organ damage, and mortality (Karki et al., 2021). In addition, increased CXCL-10 expression is closely associated with type 1 diabetes mellitus (He et al., 2015), which may be one reason for the higher increase in CXCL-10 levels in hACE2-Lepr$^{-/-}$ mice compared to hACE2-Lepr$^{+/+}$ mice. In contrast, IFN-γ showed a greater increase in hACE2-Lepr$^{+/+}$ mice after SARS-CoV-2 infection. This suggests that blood glucose can regulate immune activity, consistent with previous studies showing that hyperglycemia

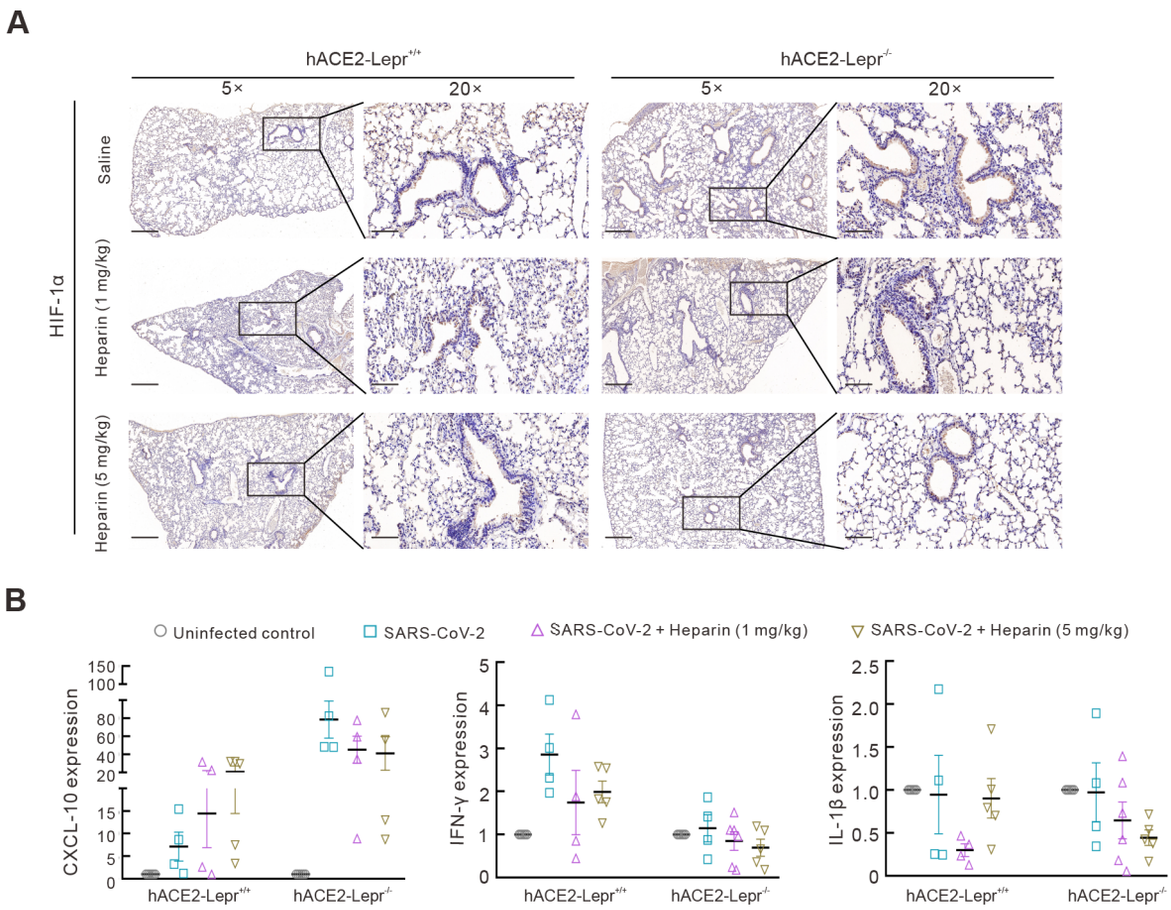

Figure 4 Mechanism of heparin blocking SARS-CoV-2 infection in diabetic models

A: IHC assay of HIF-1α in lungs of hACE2-Lepr$^{-/-}$ and hACE2-Lepr$^{+/+}$ mice treated with heparin after infection. 5×, scale bar represents 300 μm; 20×, scale bar represents 100 μm. B: mRNA levels of CXCL-10, IFN-γ, and IL-1β cytokines in lungs of hACE2-Lepr$^{-/-}$ and hACE2-Lepr$^{+/+}$ mice treated with heparin by qPCR.

affects immune functions and inflammatory responses, leading to more severe and potentially fatal outcomes in COVID-19 patients (Lim et al., 2021; Mehta et al., 2020; Zhang et al., 2020b).

While analysis of clinical data suggests an association between heparin administration and reduced mortality in COVID-19 patients (De Vito et al., 2023), the pharmacological effects and underlying mechanisms remain unclear. As hACE2-Lepr$^{-/-}$ effectively simulated severe COVID-19, we systematically examined the antiviral effects of heparin in hACE2-Lepr$^{+/+}$ mice and the combined effects of heparin-insulin in hACE2-Lepr$^{-/-}$ mice. After heparin administration, particularly at high doses, both mouse models exhibited marked improvement, with decreased viral titers, histopathological changes, dyspnea, and inflammatory factor secretion, supporting the use of heparin for the treatment of COVID-19 patients. Our results showed that heparin limited disease progression, likely by inhibiting HIF-1α expression and related inflammatory responses (Li et al., 2020). Hypercoagulative status and microthrombosis, which are associated with respiratory distress and hypoxia, are two important characteristics of diabetic patients with COVID-19 (Landstra & De Koning, 2021). Thus, the ameliorative effects of heparin on dyspnea may stem from its ability to alleviate the hypercoagulative status in patients with COVID-19. Furthermore, heparin may prevent SARS-CoV-2 invasion by affecting electrostatic interactions between the heparan sulfate proteoglycans and SARS-CoV-2 S protein, an essential factor in hACE2-mediated invasion of SARS-CoV-2 into target cells (Kearns et al., 2022; Zhang et al., 2022b).

The combined use of heparin and insulin, which can regulate both blood glucose levels and disease progression, was effective for treating hACE2-Lepr$^{-/-}$ mice, suggesting that these drugs could be used in COVID-19 patients with diabetes. Results showed that blood glucose levels decreased after insulin treatment but rebounded by 3 dpi. This pattern resembles the ketoacidosis observed in diabetic patients, potentially attributable to impaired pancreatic ducts and islets due to direct SARS-CoV-2 infection (Coate et al., 2020), leading to hyperglycemia driven by excitability (Khunti et al., 2021).

Our study has several limitations. As this was a retrospective cohort study, diabetes was not subtyped at admission, reducing the comprehensiveness of results. In addition, although we adjusted for many confounding factors in the multivariate logistic regression analysis, unknown or unmeasured variables may have influenced the mortality and complications observed in COVID-19 patients. Furthermore, the patient sample size was relatively small, suggesting the need for validation with larger samples or multi-center data. The animal experiments also had limitations. The number of hACE2-Lepr$^{-/-}$ mice and experimental conditions restricted the consistent grouping of mice, and LMWH doses were not examined using a dose-dependent study. Although HIF-1α, a hypoxia marker, was identified as an important factor post SARS-CoV-2 infection in the animal experiments, infected

mice were not treated with a HIF-1α inhibitor, which should be performed in future animal models and clinical studies to develop treatment strategies against SARS-CoV-2 infections.

In conclusion, two SARS-CoV-2-infected mouse models, hACE2-Lepr$^{-/-}$ and hACE2-HFD mice, mimicking the complex pathological states of COVID-19 patients with diabetes and obesity, were developed. Based on animal experiments and previous clinical data (Khunti et al., 2021; Lim et al., 2021), combined hypoglycemic and anticoagulant therapy is recommended for treating COVID-19 patients with diabetes, particularly in critical cases. Furthermore, preventive administration of anticoagulant therapy should be considered in aged people with diabetes in the context of SARS-CoV-2 management.

ACKNOWLEGEMENTS

We thank the staff members of the ABSL-3 of Institute of Microbiology, Chinese Academy of Science for technical support and assistance.

SUPPLEMENTARY DATA

Supplementary data to this article can be found online.

COMPETING INTERESTS

The authors declare that they have no competing interests.

AUTHORS' CONTRIBUTIONS

Y.B., J.W. conceived the concept; Y.B., J.W., and N.Z. designed the study and analyzed the data; N.Z., Z.Z., J.Y., C.Z., Y.G., M.J., N.P., and X.Z. performed the experiments; X.Y. provided clinical data; M.Z., W.G., and G.N. assisted in data analysis; Z.Z. analyzed the clinical data; J.W. and Z.Z. constructed the mouse models; X.L., Q.Z., M.L., X.L., and X.S. assisted with H&E staining; Y.B., N.Z., and Z.Z. wrote the manuscript; Y.B., J.W., X.L., N.Z., Z.Z., G.N., and G.G. revised the manuscript. All authors read and approved the final version of the manuscript.

REFERENCES

Abdelmassih A, Yacoub E, Husseiny RJ, et al. 2021. Hypoxia-inducible factor (HIF): The link between obesity and COVID-19. *Obesity Medicine*, **22**: 100317.

Abdi M, Lamardi ZH, Shirjan F, et al. 2022. The Effect of aspirin on the prevention of pro-thrombotic states in hospitalized COVID-19 patients: systematic review. *Cardiovascular & Hematological Agents in Medicinal Chemistry*, **20**(3): 189−196.

Abou-Ismail MY, Diamond A, Kapoor S, et al. 2020. The hypercoagulable state in COVID-19: Incidence, pathophysiology, and management. *Thrombosis Research*, **194**: 101−115.

Abrignani MG, Murrone A, De Luca L, et al. 2022. COVID-19, vaccines, and thrombotic events: a narrative review. *Journal of Clinical Medicine*, **11**(4): 948.

Arce VM, Costoya JA. 2021. SARS-CoV-2 infection in K18-ACE2 transgenic mice replicates human pulmonary disease in COVID-19. *Cellular & Molecular Immunology*, **18**(3): 513−514.

Chung M, Bernheim A, Mei XY, et al. 2020. CT imaging features of 2019 novel coronavirus (2019-nCoV). *Radiology*, **295**(1): 202−207.

Coate KC, Cha J, Shrestha S, et al. 2020. SARS-CoV-2 cell entry factors ACE2 and TMPRSS2 are expressed in the microvasculature and ducts of human pancreas but are not enriched in β Cells. *Cell Metabolism*, **32**(6): 1028−1040.e4.

Dai LP, Zheng TY, Xu K, et al. 2020. A universal design of betacoronavirus vaccines against COVID-19, MERS, and SARS. *Cell*, **182**(3): 722−733.e11.

De Vito A, Saderi L, Fiore V, et al. 2023. Early treatment with low-molecular-weight heparin reduces mortality rate in SARS-CoV-2 patients. *Panminerva Medica*, **65**(3): 286−291.

Desdiani D. 2022. Response to late diagnosis of COVID-19 and hypercoagulable state. *Canadian Journal of Respiratory Therapy*, **58**: 121.

Di Micco P, Imbalzano E, Russo V, et al. 2021. Heparin and SARS-CoV-2: multiple pathophysiological links. *Viruses*, **13**(12): 2486.

Dong SH, Liang S, Cheng ZQ, et al. 2022. ROS/PI3K/Akt and Wnt/β-catenin signalings activate HIF-1α-induced metabolic reprogramming to impart 5-fluorouracil resistance in colorectal cancer. *Journal of Experimental & Clinical Cancer Research*, **41**(1): 15.

Fan Q, Zhu HL, Zhao JX, et al. 2020. Risk factors for myocardial injury in patients with coronavirus disease 2019 in China. *ESC Heart Failure*, **7**(6): 4108−4117.

Fan WH, Sun SS, Zhang N, et al. 2022. Nasal delivery of thermostable and broadly neutralizing antibodies protects mice against SARS-CoV-2 infection. *Signal Transduction and Targeted Therapy*, **7**(1): 55.

Francistiova L, Klepe A, Curley G, et al. 2021. Cellular and molecular effects of SARS-CoV-2 linking lung infection to the brain. *Frontiers in Immunology*, **12**: 730088.

Glaser J, Gonzalez R, Sadr E, et al. 2006. Neutralization of the chemokine CXCL10 reduces apoptosis and increases axon sprouting after spinal cord injury. *Journal of Neuroscience Research*, **84**(4): 724−734.

Guan WJ, Ni ZY, Hu Y, et al. 2020. Clinical characteristics of coronavirus disease 2019 in China. *New England Journal of Medicine*, **382**(18): 1708−1720.

He JS, Lian CW, Fang YL, et al. 2015. Effect of CXCL10 receptor antagonist on islet cell apoptosis in a type I diabetes rat model. *International Journal of Clinical and Experimental Pathology*, **8**(11): 14542−14548.

Huang JL, Covic M, Huth C, et al. 2021. Validation of candidate phospholipid biomarkers of chronic kidney disease in hyperglycemic individuals and their organ-specific exploration in leptin receptor-deficient db/db mouse. *Metabolites*, **11**(2): 89.

Jafari M, Arabit JGJ, Courville R, et al. 2022. The impact of *Rhodiola rosea* on biomarkers of diabetes, inflammation, and microbiota in a leptin receptor-knockout mouse model. *Scientific Reports*, **12**(1): 10581.

Javeed N, Her TK, Brown MR, et al. 2021. Pro-inflammatory β cell small extracellular vesicles induce β cell failure through activation of the CXCL10/CXCR3 axis in diabetes. *Cell Reports*, **36**(8): 109613.

Karki R, Sharma BR, Tuladhar S, et al. 2021. Synergism of TNF-α and IFN-γ triggers inflammatory cell death, tissue damage, and mortality in SARS-CoV-2 infection and cytokine shock syndromes. *Cell*, **184**(1): 149−168.e17.

Kearns FL, Sandoval DR, Casalino L, et al. 2022. Spike-heparan sulfate interactions in SARS-CoV-2 infection. *Current Opinion in Structural Biology*, **76**: 102439.

Khunti K, Del Prato S, Mathieu C, et al. 2021. COVID-19, hyperglycemia, and new-onset diabetes. *Diabetes Care*, **44**(12): 2645−2655.

Kim JA, Kim SH, Seo JS, et al. 2022. Temporal transcriptome analysis of SARS-CoV-2-infected lung and spleen in human ACE2-transgenic mice. *Molecules and Cells*, **45**(12): 896−910.

Kouidere A, El Youssoufi L, Ferjouchia H, et al. 2021. Optimal Control of Mathematical modeling of the spread of the COVID-19 pandemic with highlighting the negative impact of quarantine on diabetics people with Cost-effectiveness. *Chaos, Solitons & Fractals*, **145**: 110777.

Landstra CP, De Koning EJP. 2021. COVID-19 and diabetes: understanding the interrelationship and risks for a severe course. *Frontiers in Endocrinology*, **12**: 649525.

Lei JQ, Li JF, Li X, et al. 2020. CT imaging of the 2019 novel coronavirus (2019-nCoV) pneumonia. *Radiology*, **295**(1): 18.

Li LF, Liu YY, Lin SW, et al. 2020. Low-molecular-weight heparin reduces ventilation-induced lung injury through hypoxia inducible factor-1α in a murine endotoxemia model. *International Journal of Molecular Sciences*, **21**(9): 3097.

Liang Y, Li H, Li J, et al. 2020. Role of neutrophil chemoattractant CXCL5 in

SARS-CoV-2 infection-induced lung inflammatory innate immune response in an in vivo hACE2 transfection mouse model. *Zoological Research*, **41**(6): 621−631.

Lim S, Bae JH, Kwon HS, et al. 2021. COVID-19 and diabetes mellitus: from pathophysiology to clinical management. *Nature Reviews Endocrinology*, **17**(1): 11−30.

Lima-Martinez MM, Boada CC, Madera-Silva MD, et al. 2021. COVID-19 and diabetes: A bidirectional relationship. *Clínica e Investigación en Arteriosclerosis*, **33**(3): 151−157.

Litov L, Petkov P, Rangelov M, et al. 2021. Molecular mechanism of the anti-Inflammatory action of heparin. *International Journal of Molecular Sciences*, **22**(19): 10730.

Magiorkinis G. 2023. On the evolution of SARS-CoV-2 and the emergence of variants of concern. *Trends in Microbiology*, **31**(1): 5−8.

Mehta P, Mcauley DF, Brown M, et al. 2020. COVID-19: consider cytokine storm syndromes and immunosuppression. *Lancet*, **395**(10229): 1033−1034.

Merad M, Blish CA, Sallusto F, et al. 2022. The immunology and immunopathology of COVID-19. *Science*, **375**(6585): 1122−1127.

Nguyen JL, Alfred T, Reimbaeva M, et al. 2022. Population attributable fractions of underlying medical conditions for coronavirus disease 2019 (COVID-19) diagnosis and COVID-19 hospitalizations, ventilations, and deaths among adults in the United States. *Open Forum Infectious Diseases*, **9**(5): ofac099.

O'donnell KL, Pinski AN, Clancy CS, et al. 2021. Pathogenic and transcriptomic differences of emerging SARS-CoV-2 variants in the Syrian golden hamster model. *eBioMedicine*, **73**: 103675.

Oliveira S, Monteiro-Alfredo T, Henriques R, et al. 2022. Improvement of glycaemia and endothelial function by a new low-dose curcuminoid in an animal model of type 2 diabetes. *International Journal of Molecular Sciences*, **23**(10): 5652.

Ou XT, Lv WB. 2020. Metabolic changes and interaction of tumor cell, myeloid-derived suppressor cell and T cell in hypoxic microenvironment. *Future Oncology*, **16**(8): 383−393.

Pascarella G, Strumia A, Piliego C, et al. 2020. COVID-19 diagnosis and management: a comprehensive review. *Journal of Internal Medicine*, **288**(2): 192−206.

Petelina TI, Musikhina NA, Garanina VD, et al. 2022. Characterization of blood biomarkers in prospective follow-up of patients with cardiovascular pathology in combination with type 2 diabetes mellitus after COVID-19 associated pneumonia. *Klinicheskaia Laboratornaia Diagnostika*, **67**(10): 561−569.

Polidoro RB, Hagan RS, De Santis Santiago R, et al. 2020. Overview: systemic inflammatory response derived from lung injury caused by SARS-CoV-2 infection explains severe outcomes in COVID-19. *Frontiers in Immunology*, **11**: 1626.

Ramos-Guzman CA, Ruiz-Pernia JJ, Tuñón I. 2021. Inhibition mechanism of SARS-CoV-2 main protease with ketone-based inhibitors unveiled by multiscale simulations: insights for improved designs. *Angewandte Chemie International Edition*, **60**(49): 25933−25941.

Rui F, Jiawei K, Yuntao H, et al. 2021. Undenatured type II collagen prevents and treats osteoarthritis and motor function degradation in T2DM patients and db/db mice. *Food & Function*, **12**(10): 4373−4391.

Santus P, Radovanovic D, Saderi L, et al. 2020. Severity of respiratory failure at admission and in-hospital mortality in patients with COVID-19: a prospective observational multicentre study. *BMJ Open*, **10**(10): e043651.

Shu CJ, Huang X, Tang HH, et al. 2021. Mutations in spike protein and allele variations in ACE2 impact targeted therapy strategies against SARS-CoV-2. *Zoological Research*, **42**(2): 170−181.

Singh AK, Khunti K. 2022. COVID-19 and diabetes. *Annual Review of Medicine*, **73**: 129−147.

Tang N, Li DJ, Wang X, et al. 2020. Abnormal coagulation parameters are associated with poor prognosis in patients with novel coronavirus pneumonia. *Journal of Thrombosis and Haemostasis*, **18**(4): 844−847.

The Chinese National Health Commission. 2023. Chinese Clinical Guidance for COVID-19 pneumonia diagnosis and treatment (10th version).

Tian MF, Liu WY, Li X, et al. 2021. HIF-1α promotes SARS-CoV-2 infection and aggravates inflammatory responses to COVID-19. *Signal Transduction and Targeted Therapy*, **6**(1): 308.

Toor R, Zamora FJ, Fatteh N, et al. 2021. Use of low-molecular-weight heparin and peak anti-Xa monitoring in severe SARS-CoV-2 disease: a brief report. *Hospital Pharmacy*, **56**(6): 640−645.

Verveen A, Wynberg E, Van Willigen HDG, et al. 2022. Health-related quality of life among persons with initial mild, moderate, and severe or critical COVID-19 at 1 and 12 months after infection: a prospective cohort study. *BMC Medicine*, **20**(1): 422.

Wang BJ, Vadakke-Madathil S, Croft LB, et al. 2022. HIF-1α cardioprotection in COVID-19 patients. *JACC:Basic to Translational Science*, **7**(1): 67−69.

Wang DW, Hu B, Hu C, et al. 2020. Clinical characteristics of 138 hospitalized patients with 2019 novel coronavirus-infected pneumonia in Wuhan, China. *JAMA*, **323**(11): 1061−1069.

Wang T, Zhang N, Fan SP, et al. 2021. Establishment of human distal lung organoids for SARS-CoV-2 infection. *Cell Discovery*, **7**(1): 108.

Wu ML, Liu FL, Sun J, et al. 2022. Combinational benefit of antihistamines and remdesivir for reducing SARS-CoV-2 replication and alleviating inflammation-induced lung injury in mice. *Zoological Research*, **43**(3): 457−468.

Zepeda AB, Pessoa A Jr, Castillo RL, et al. 2013. Cellular and molecular mechanisms in the hypoxic tissue: role of HIF-1 and ROS. *Cell Biochemistry and Function*, **31**(6): 451−459.

Zhang JJ, Dong X, Cao YY, et al. 2020a. Clinical characteristics of 140 patients infected with SARS-CoV-2 in Wuhan, China. *Allergy*, **75**(7): 1730−1741.

Zhang Y, Xiao M, Zhang SL, et al. 2020b. Coagulopathy and antiphospholipid antibodies in patients with Covid-19. *The New England Journal of Medicine*, **382**(17): e38.

Zhang YL, Sun YY, Liu K, et al. 2021. Low plasma angiotensin-converting enzyme 2 level in diabetics increases the risk of severe COVID-19 infection. *Aging*, **13**(9): 12301−12307.

Zhang YP, Luo W, Li Q, et al. 2022a. Risk factors for death among the first 80 543 coronavirus disease 2019 (COVID-19) cases in China: relationships between age, underlying disease, case severity, and region. *Clinical Infectious Diseases*, **74**(4): 630−638.

Zhang ZY, Zhang J, Wang JQ. 2022b. Surface charge changes in spike RBD mutations of SARS-CoV-2 and its variant strains alter the virus evasiveness *via* HSPGs: A review and mechanistic hypothesis. *Frontiers in Public Health*, **10**: 952916.

Zhou F, Yu T, Du RH, et al. 2020a. Clinical course and risk factors for mortality of adult inpatients with COVID-19 in Wuhan, China: a retrospective cohort study. *The Lancet*, **395**(10229): 1054−1062.

Zhou P, Yang XL, Wang XG, et al. 2020b. A pneumonia outbreak associated with a new coronavirus of probable bat origin. *Nature*, **579**(7798): 270−273.

Zhu N, Wang WL, Liu ZD, et al. 2020. Morphogenesis and cytopathic effect of SARS-CoV-2 infection in human airway epithelial cells. *Nature Communications*, **11**(1): 3910.